Naval Research Laboratory

Washington, DC 20375-5320

NRL/MR/6041--20-10,191

Large-Eddy Simulations of Nozzle-Exit Conditions in Subsonic Jet Flows

Junhui Liu

Laboratories for Computational Physics and Fluid Dynamics Branch
Materials Science & Component Technology Division

October 26, 2020

REPORT DOCUMENTATION PAGE

Form Approved
OMB No. 0704-0188

1. REPORT DATE *(DD-MM-YYYY)*	**2. REPORT TYPE**	**3. DATES COVERED** *(From - To)*
26-10-2020	NRL Memorandum Report	September 2019 – September 2020

4. TITLE AND SUBTITLE

Large-Eddy Simulations of Nozzle-Exit Conditions in Subsonic Jet Flows

5a. CONTRACT NUMBER

5b. GRANT NUMBER

5c. PROGRAM ELEMENT NUMBER

6. AUTHOR(S)

Junhui Liu

5d. PROJECT NUMBER

5e. TASK NUMBER

5f. WORK UNIT NUMBER
1L64

7. PERFORMING ORGANIZATION NAME(S) AND ADDRESS(ES)

Naval Research Laboratory
4555 Overlook Avenue, SW
Washington, DC 20375-5320

8. PERFORMING ORGANIZATION REPORT NUMBER

NRL/MR/6041--20-10,191

9. SPONSORING / MONITORING AGENCY NAME(S) AND ADDRESS(ES)

Naval Research Laboratory
4555 Overlook Avenue, SW
Washington, DC 20375-5320

10. SPONSOR / MONITOR'S ACRONYM(S)

11. SPONSOR / MONITOR'S REPORT NUMBER(S)

12. DISTRIBUTION / AVAILABILITY STATEMENT

DISTRIBUTION STATEMENT A: Approved for public release; distribution is unlimited.

13. SUPPLEMENTARY NOTES

14. ABSTRACT

Large-eddy simulations have been used to simulate the nozzle-exit conditions of subsonic jet flows generated by three types of nozzles. The wall-model approach is used to account for the nozzle boundary-layer effect. The nozzles involved in this study are all related to the SMC000 nozzle tested extensively at NASA Glenn Research center. The nozzle-exit profiles are comparable to those measured in experiments using the similar nozzle geometries. To investigate the boundary-layer state on the nozzle-exit conditions, pipe extensions are attached to the SMC000 nozzle to generate nozzle-exit boundary layers in laminar, transitional and turbulent states. It is found that the downstream jet plume affects the nozzle-exit boundary-layer development, causing the boundary-layer transition occurs earlier than that observed inside a pipe. The nozzle-exit boundary layers in the transitional state involve significantly larger turbulence intensities, similar to those observed in highly disturbed but nominally laminar boundary layers shown in experiments. This may indicate that those highly disturbed nominally laminar boundary layers are in the transitional state.

15. SUBJECT TERMS

CFD, Large-eddy simulations, Jet noise, Subsonic jet flows, Boundary-layer state, Nozzle-exit conditions, Nozzle flows

16. SECURITY CLASSIFICATION OF:			**17. LIMITATION OF ABSTRACT**	**18. NUMBER OF PAGES**	**19a. NAME OF RESPONSIBLE PERSON**
a. REPORT	**b. ABSTRACT**	**c. THIS PAGE**			Junhui Liu
Unclassified Unlimited	Unclassified Unlimited	Unclassified Unlimited	Unclassified Unlimited	21	**19b. TELEPHONE NUMBER** *(include area code)* (202) 767-6590

This page intentionally left blank.

CONTENTS

This page intentionally left blank.

EXECUTIVE SUMMARY

Large-eddy simulations have been used to simulate the nozzle-exit conditions in subsonic jet flows generated by three types of nozzles. The wall-model approach is used to account for the nozzle boundary-layer effect. The nozzles involved in this study are all related to the SMC000 nozzle tested extensively at NASA Glenn Research center. The nozzle-exit profiles are comparable to those measured in experiments using similar nozzle geometries. Both numerical predictions and laboratory measurements present a similar peak intensity with different upstream boundary-layer conditions. This suggests that the turbulence intensity level at the nozzle exit is more sensitive to the contraction ratio near the nozzle exit than to the upstream boundary-layer turbulence conditions. To investigate the boundary-layer state on the nozzle-exit conditions, several pipe extensions are attached to the SMC000 nozzle to generate nozzle-exit boundary layers in laminar, transitional and turbulent states. It is found that the downstream jet plume affects the nozzle-exit boundary-layer development, causing the boundary-layer transition occurs earlier than the boundary-layer transition observed inside a pipe. The nozzle-exit boundary layers in the transitional state involve significantly larger turbulence intensities, similar to those observed in highly disturbed but nominally laminar boundary layers shown in experiments. This may indicate that those highly disturbed nominally laminar boundary layers are in the transitional state. However, noise data are needed to confirm this claim.

This page intentionally left blank.

Large-Eddy Simulations of Nozzle-Exit Conditions in Subsonic Jet Flows

1. INTRODUCTION

It has been observed in various experiments that a nozzle with a large contraction ratio often generates higher high-frequency noise intensity than that of a nozzle with a small contraction ratio (Refs [1]-[3]). The noisier one was found to involve a highly disturbed but nominally laminar boundary layer at the nozzle exit, on the other hand, the quieter nozzle had a turbulent boundary layer. The nominally laminar boundary layer was found to involve significantly larger turbulence intensities that correlate with higher noise radiation. This is often referred as the effect of the nozzle initial condition. This effect has been also investigated by numerical approaches (Refs [4]-[5]).

The current NASA's Commercial Supersonic Technology (CST) project requires high-fidelity jet noise prediction capabilities for exhaust flows operating at subsonic takeoff conditions. The large-eddy simulation flow solver JENRE® developed at NRL has been frequently applied to the simulations of supersonic jet flows and the noise generation [Refs [6]-[9]] in the past decade, but less work has been performed on jet flows operating at subsonic conditions. The first numerical effort using JENRE® code to simulate subsonic jet flows was presented in Ref. [10], where the jet plume quantities were compared with experimental data and a good agreement was observed. The current report is the second paper that documents the numerical effort using JENRE® to simulate subsonic jet flows but with a focus on the nozzle-exit conditions. In this work, three types of nozzles are used. The first is the SMC000 nozzle (Figure 1(a)), which has been used extensively in investigations of noise and flow-field characteristics of isolated jets as well as various complex flow configurations (Refs [10]-[17]). The second nozzle has a 12” pipe attached upstream of the final convergent section of SMC00 nozzle, as shown in Figure 1(b). Some experimental and numerical investigations using this second nozzle can be found in Refs [14] and [17]. The third type of nozzle has a pipe attached to the SMC000 nozzle and various pipe lengths have been used (Figure 1(c)) to investigate the effect of the boundary-layer state on the nozzle-exit profiles.

2. COMPUTATIONAL METHODOLOGY AND SIMULATION SETUP

JENRE® code is built on a general framework that includes support for different types of numerics, including cell-centered finite volume and nodal finite element methods. In the current jet noise simulations, we use the nodal Taylor-Galerkin finite element flow solver because of its two advantages over the standard cell-centered finite-volume approach. First, Taylor-Galerkin finite element method maintains the second order spatial accuracy even on tetrahedral cells, so its accuracy is more consistent than that of the finite volume approach. The finite volume approach is sensitive to cell types and can be rather dissipative on tetrahedral mesh. The tetrahedral mesh, however, is often the preferred mesh type when complex geometries are involved. The second advantage is that the nodal method requires less computational memory than the cell-centered method because it requires a smaller number of degrees of freedom. In the current Taylor-Galerkin finite element flow solver, the finite element flux corrected transport (FEM-FCT) method is used for the flux integration and limiting calculations (Refs [18]-[19]). The multi-dimensional FCT flux limiter provides an implicit subgrid stress model, and the methodology is in the category of the Monotonically Integrated Large-Eddy Simulation approach. The tetrahedral mesh is used because of its simplicity and the accurate representation of complex geometries. In addition, a wall-model method based on the equilibrium wall model is implemented in JENRE® to account for the boundary-layer effect inside the nozzle [9].

Manuscript approved October 16, 2020.

The nozzle-exit diameters (D) are 2" in all three types of nozzles shown in Figure 1. The cell-size distribution outside the nozzle is controlled by the control points shown in this figure. The cell size at each control point is shown in Table 1. The cell size in the axial direction follows a linear distribution, but it follows an exponential distribution in the radial direction. The cell size is D/400 adjacent to the nozzle surface to account for the boundary-layer effect, where D is the nozzle-exit diameter.

3. RESULTS AND DISCUSSIONS

Simulations have been carried out to simulate the flow inside and outside the three types of nozzles. A clean flow is used at each nozzle inlet, and boundary-layer tripping in the form of the surface roughness is used in some simulations to introduce turbulences inside the nozzle boundary layer. Effects of the surface roughness and the boundary-layer state on nozzle-exit radial profiles of the axial velocity and turbulence intensity are examined and the results are quantitively compared with experimental data (Ref. [16]). The nozzle-exit profiles are measured slightly downstream at x/D = 0.015D to match the location used in measurements (Ref. [16]).

3.1 SMC000 nozzle

As shown in Figure 1(a), the axial length of this nozzle geometry is short and there is a favorable pressure gradient introduced by the nozzle convergent contours. Since a clean inlet flow could result a very thin and very likely laminar boundary layer at the nozzle exit, a boundary-layer tripping using the surface roughness , as shown in Figure 3, is added to the nozzle surface prior to one diameter upstream of the nozzle exit. Four surface roughness heights are tested and the roughness height ranges from 1.0E-03" to 5.6E-04", as shown in Figure 4(a). The acoustic Mach number is M_a = 0.7 and the jet Mach number M_j is 0.736. The acoustic Mach number M_a is the ratio between the velocity and the ambient sound speed and the jet Mach number M_j is the Mach number when the jet is fully expanded.

It can be seen that the peak turbulence intensity is not sensitive to the roughness height when the roughness height is sufficient large. In this figure, only the turbulence intensity is substantially lower with the smallest roughness height. Increasing the roughness height broadens the turbulence intensity profiles. It can be also seen that there is a good agreement between the predicted peak intensities and the peak intensity measured at M_j = 0.685 shown in Ref. [16]. However, the predicted mean profile shows a thinner shear layer that the maximum U/U_j reaches at Y/D = 0.49 but the measured profile reaches the maximum at Y/D = 0.476). U_j is the fully expanded jet velocity. This indicates that the nozzle boundary layers predicted in the simulations are much thinner. The slightly higher Mach number used in these numerical simulations may contribute to this thinner shear layer to some extent. In addition, the predicted intensity u'/U_j peak locations are slightly further into the jet center that the predicted intensity reaches peak at Y/D = 0.492 but the measured peak of u'/U_j is at Y/D = 0.496). Since the cell size adjacent to the wall is only D/400, there are only 1.6 cells between the peak location of Y/D = 0.496 and the nozzle surface and three cells between Y/D = 0.492 and the nozzle surface. It can be seen that the grid resolution used in simulations is extremely coarse in terms of the boundary-layer simulations. Our previous experience shows that increasing the grid resolution near the wall will help to shift the peak location towards the wall (Ref. [9]).

Figure 5 shows the centerline distributions of the axial velocity and the turbulence intensity distributions on both centerline and lip line. The small differences shown in the nozzle-exit profiles affect slightly the jet core length. In the predictions using the three larger roughness heights, the jet core length increases slightly as the roughness height increases. However, the prediction using the smallest roughness does not follow this trend. The peak intensity near the nozzle lip decreases slightly from u'/U_j = 0.19 to 0.18 as the roughness height increases. It can be seen that there is a rapid increase of the turbulence intensity from the nozzle exit to x/D = 0.5 before settling to roughly 0.14 in the downstream shear layer. And this is relatively independent of the roughness heights used for the boundary-layer

tripping in the nozzle. This rapid increase of the turbulence intensity indicates that there is a transition from the nozzle boundary layer to the downstream turbulent shear layer. This should include the contribution of the turbulence structures transition from a favorable pressure gradient condition inside the nozzle to the zero-pressure gradient condition inside the shear layer. Since the nozzle boundary layers in the simulations are probably only disturbed laminar boundary layers, the transition could also include the contribution of the transition from the nozzle laminar boundary layer to the downstream turbulent shear layer.

In addition, the effect of the jet Mach number on the nozzle exit profiles are shown in Figure 6, where the roughness of 5.9E-04" is used. It can be seen that the effect on the peak intensity is also small, but a lower Mach number generates a thicker boundary layer and a broader turbulence intensity profile. This probably is due to the Reynolds-number effect that the viscous effect is larger when the Reynolds number is small. The difference between the two higher Mach numbers is small, and this may indicate that a Reynolds-number similarity can be established if the Reynolds number is sufficient large.

3.2 Nozzle with a 12" pipe upstream of the final convergent section

This nozzle has a12" pipe connected to the final convergent section of SMC000 nozzle. This extra upstream pipe helps to generate a fully developed boundary layer upstream of the final convergent section. This provides a more realistic nozzle-exit boundary-layer condition than those shown in above. Figure 7(a) shows the axial velocity contours near the nozzle surface inside the pipe. It can be seen that the nozzle flow has gone through laminar, transitional and turbulent stages. Since the wall shear stress is computed from the fully developed velocity profile in the equilibrium wall model, the wall shear stress may have been overestimated in the laminar and the early transition regions and this may have caused the transition occur slightly early. But since the transition location also depends on the nozzle surface condition and the upstream turbulences, its exact location is not easily to be determined. The trend of the boundary-layer development, however, is consistent. In the transition region, the turbulence structures are initially in a ring shape, but they break down and eventually evolve to streak structures in the turbulent boundary layer region. The peak turbulent intensity is found in this transition region between 3D and 4D upstream of the nozzle exit as shown in Figure 7(b). Two turbulent intensity profiles inside the pipe at x = -3.4D and x = -1.0D are presented along with the profile near the nozzle exit (x = 0.015D) in Figure 7(c). The location of x = -3.4D is in the boundary-layer transition region, where the turbulent intensity reaches its peak value near $0.9U_j$. On the other hand, the location of x = -1.0D is in the fully developed boundary-layer region. The turbulence intensity at the fully developed location is lower than the peak intensity, but the profile is much broader due to the thicker boundary layer. The intensity near the nozzle exit is further reduced and this is due to the favorable pressure gradient presented in the convergent section.

If the boundary-layer tripping is added upstream of the pipe, the transitional and turbulent stages start further upstream as shown in Figure 8. The peak intensity location is around x = -4.8D. The intensity profiles at the fully developed location of x = -1D and the profile at the nozzle exit are broader than those where no upstream boundary-layer tripping is used. This can be seen in Figure 7(c). These broader profiles should be associated with a thicker boundary layer at the end of the pipe. When the boundary-layer tripping is used, the turbulent boundary layer inside the pipe starts further upstream and this gives a longer axial distance for the boundary-layer development. The nozzle-exit profiles are compared with the experimental data as shown in Figure 9. It can be seen that the overall agreement is good, but the profiles with boundary-layer tripping appear to have a better agreement with experimental data. The overall agreement between the predicted profiles and the measured profiles is better than that shown in Figure 4. It is also interesting to see that the peak intensity is not sensitive to the upstream boundary-layer tripping. Figure 10 compares the nozzle-exit velocity and turbulence intensity profiles generated by the SMC000 nozzle with those generated by the nozzle with 12" upstream of the final convergent section. An upstream boundary-layer tripping in the form of a surface

roughness with the height of 5.9E-04" is used in the simulation where the SMC000 nozzle is used. A boundary-layer tripping is also used upstream of the 12" pipe in the simulation where the extra pipe is added. The extra 12" pipe upstream of the final convergent section produces a much thicker boundary layer, which increases the momentum deficit. This generates a broader turbulence intensity profile, but the peak intensity remains similar. This may suggest that the peak intensity is more sensitive to the contraction ratio of the final convergent section than the upstream turbulence conditions inside the nozzle boundary layer.

As shown in Figure 4, the velocity in the jet core near the nozzle exit is slightly smaller than the jet velocity in both simulations. This is because the radial profile of the nozzle-exit pressure does not immediately become uniform and match the ambient pressure. It takes a small axial distance further downstream to fully match the ambient pressure. This will be discussed in further details in the following subsection. Figure 11 compares the axial distributions of the velocity and turbulence intensity between these two simulations. The difference between the jet core lengths is small, but the peak turbulence intensity near the nozzle lip is lower in the simulation where the extra pipe is used. This difference may be contributed by two sources. The first is the physical source. The nozzle boundary layer inside the SMC000 nozzle with an upstream tripping and clean inlet flow may be only disturbed laminar boundary layer, but the boundary layer inside the nozzle with 12" pipe added upstream of the final convergent section is clearly in turbulent state. Thus, the transition from the turbulent boundary layer to the turbulent shear layer should be much smother and less turbulent energy should be generated due to the transition. The second is due to the relatively finer grid resolution used for the boundary layer simulation. Since the grid resolution for the nozzle boundary layer is similar in both simulations, the simulation with the extra pipe has a relatively finer grid resolution because of the thicker boundary layer. This relatively finer grid resolution should be able to capture more turbulence structures if they are available.

These two factors both physical and numerical will help to produce a fuller spectrum of turbulence structures than that uses a simple SMC000 nozzle. As shown in Figure 7 and Figure 8, the boundary-layer transition from laminar to turbulent inside the pipe always produces high turbulence intensity. It is expected that the transition from the nozzle boundary layer with a fuller spectrum of the turbulence structures to the turbulent shear layer would be relatively smoother, and the turbulence intensity contributed by the transition would be less. This in turn will produce a smaller peak intensity downstream of the nozzle lip. Thus, the transition from a laminar boundary layer to the turbulent shear layer should generate the highest peak intensity near the nozzle lip, but the transition from a fully resolved and fully developed turbulent boundary layer to the turbulent shear layer is expected to be very smooth and no peak intensity would be observed. In numerical simulations, however, even when the nozzle boundary layer is supposed to be turbulent, an insufficient grid resolution will not resolve all small turbulent scales near the nozzle wall and the spectrum of turbulence structures cannot be fully predicted. Thus, the transition from this unresolved turbulent boundary layer to the downstream shear layer will not as smooth as that observed in the transition from the fully resolved turbulent boundary layer to the downstream shear layer. The peak intensity along the lip line downstream of the nozzle exit will depend on the grid resolution used inside the nozzle turbulent boundary layer.

3.3 SMC000 nozzle with a pipe extension

As shown in Figure 7 and Figure 8, the turbulence structures in the transition region of the nozzle boundary layer differ from those in the fully developed boundary-layer region, and the turbulence intensity is higher in the transition region. It would be useful to examine the effect of the boundary-layer state on the nozzle-exit profiles. It is not easy to carry out this task by using the SMC000 nozzle alone because it requires a good control of the inlet turbulences in the simulations. Thus, pipe extensions are attached to the SMC000 nozzle to generate boundary layers at various boundary-layer state at the nozzle exit. A pipe extension of 6D is first used to examine the possible transition location in the pipe

as shown in Figure 13. No upstream boundary-layer tripping is used in this investigation. It can be seen that the peak intensity region is around 3D downstream of the pipe inlet. Thus, a 3D pipe extension is used as shown in Figure 13. However, it appears that the interaction between the downstream jet plume affects the boundary-layer development at the nozzle exit. The peak intensity shifts upstream by 0.5D. Velocity and turbulence intensity profiles are examined at three axial locations: x = -1D, x = -0.5D and the location near the nozzle exit. The turbulence intensity at x = -1.0D is low and this location is clearly in the laminar region. The intensity reaches the peak at x = -0.5D, indicating that the boundary layer is in the transitional state at this location. The intensity near the nozzle exit is lower and the profile is broader. The boundary layer at the nozzle exit could be at the late stage of the transition or already in the fully developed turbulent region. The boundary-layer shaper factor should be a good indication of the boundary-layer state, but this factor is difficult to estimate in the wall-model approach because a large portion of the boundary layer is in the first cell adjacent to the wall and the flow in the first cell is already assumed to be fully turbulent by the wall model. As discussed in Ref. [9], the shape factor computed from the linear distribution in the first cell would be very different from that computed from the logarithmic distribution. Thus, to access if the boundary layer is in transitional state can be only roughly estimated. To generate a transitional boundary layer at the nozzle exit, two more pipe extensions with 2D and 2.5D are further tested. The comparison of the nozzle-exit profiles is shown in Figure 14. It can be seen that the turbulence intensity at the nozzle exit of the 2D pipe extension is much higher than the turbulence intensity at x = -1.0D in the simulation of the 3D pipe extension, although both locations are 2D downstream of the pipe inlet. Again, this shows that the downstream jet plume affects the boundary-layer state near the nozzle exit. The peak intensity of the nozzle exit is highest with the pipe extension of 2.5D. The nozzle-exit profiles suggest that the nozzle-exit boundary layers with the extension pipe of both 2D and 2.5D should be in the transitional state.

The nozzle-exit profiles generated by five pipe extensions are presented in Figure 15. Since no boundary-layer tripping is used for all cases, the boundary layer at the nozzle exit with 1D pipe extension is laminar and the turbulence disturbance level is very low. As the pipe length is increased to 2D, the nozzle-exit boundary-layer thickness increases and the momentum deficit increases. The velocity slope near the lip line (Y/D = 0.5D) also decreases slightly, indicating that the surface shear stress decreases as the pipe length increases. But there is a sudden change of the velocity slope from the extension pipe of 2.0D to that of 2.5D, indicating a sudden increase of the surface shear stress near the nozzle exit. As shown in the classical textbooks regarding the boundary-layer development on either a flat plate or in a pipe (Refs [20]-[21]), there is a sudden increase of surface friction when the boundary layer transitions to turbulent. This is very likely that the boundary layer at the nozzle exit with the extension of 2D is in the early transition region and the pipe extension of 2.5D could be in the late transition. This is confirmed by the high peak intensities of these two cases shown in Figure 15(b). On the other hand, the peak intensities of more developed boundary layers are lower and the peak intensity converges to roughly $0.08U_j$, such as those generated by the extension pipes of 3D and 6D. The nozzle-exit radial profiles produced by the pipe extension of 2D and 2.5D are similar to those produced by so called "highly disturbed but nominally laminar boundary layer" as shown in Ref. [15], because they all involve significantly larger turbulence intensities. Figure 16(a) shows centerline distributions of the axial velocity generated by the five pipe extensions. The jet core lengths generated by the pipe extension from 1D to 2.5D are similar. The jet core length generated by the pipe extension of 3D is slightly longer, and this probably is due to the more developed turbulent boundary layer at the nozzle exit. However, the pipe extension of 6D generates the shortest jet core length. The cause of this difference is not clear so far. Figure 16(b) shows the turbulence intensities along the lip line and also the centerline. It can be seen that the axial location of the lip-line peak intensity generated by the pipe extension of 1D is further downstream than those generated by the longer pipe extensions. This is due to the longer axial distance required for the transition from the laminar boundary layer to the turbulent shear layer. In addition, the peak intensity reduces as the pipe extension length increases. As discussed above, this probably is due to the difference in the spectrum between a transitional boundary layer and a more fully developed

boundary layer and also partly due to the relatively finer grid resolution as the boundary layer gets thicker. Both factors will help to generate a fuller spectrum of resolved turbulent structures, and thus, the transition would be smoother and a lower peak intensity would be observed.

Finally, we would like to examine the effect of the convergent section on the nozzle-exit profiles by comparing the results given by the nozzle with 12" pipe placed upstream of the final convergent section and those given by the nozzle with the 12" pipe attached at the end. Figure 17 shows the comparison of the turbulence intensity contours and the nozzle-exit profiles given by these two nozzle configurations. No upstream boundary layer tripping is used for both cases. The boundary-layer transition locations are similar in these two cases that they are roughly 3D downstream of the pipe inlet. The downstream convergent section clearly reduces the boundary layer thickness. The peak turbulence intensity at the nozzle exit is suppressed by almost half. In addition, it can be seen that there are some differences between the velocities at the boundary-layer edge (or in the jet core) predicted by these two simulations. The velocity predicted by the simulation where the pipe extension is attached downstream is closer to the fully expanded jet velocity. As mentioned above, this difference should be associated with the difference in the nozzle-exit pressure profile. This can be seen in Figure 17(d), where the nozzle-exit pressure of the simulation with a pipe attached downstream is more uniform and the magnitude is closer to the ambient value. On the other hand, the simulation with the convergent nozzle produces a parabolic profile and the pressure at the core is roughly 6% higher. Thus, the velocity at the nozzle exit should be slightly lower than the jet velocity because of the higher pressure. It will take a small downstream distance to allow the pressure match the ambient value and thus the velocity match the jet velocity as shown in Figure 5(a) and Figure 11(a).

4. CONCLUSIONS

The nozzle-exit profiles of subsonic jet flows have been examined by large-eddy simulations using the wall-model approach. Three types of nozzles have been used to investigate effects of the nozzle geometry and the boundary-layer state on the nozzle-exit profiles. The nozzles involved in this study are all based on the SMC000 nozzle tested extensively at NASA Glenn Research center. Various upstream conditions have been tested, such as those generated by boundary-layer tripping in the form of nozzle surface roughness or a 12" pipe placed upstream of the final convergent section. The nozzle-exit profiles generated by these nozzle geometries are comparable to those measured in experiments. The current simulations appear to suggest that the peak intensity is more sensitive to the contract ratio near the nozzle exit than the upstream turbulence conditions. It is found that the boundary layer inside the 12" pipe goes through laminar, transitional and turbulent states. The peak turbulent intensity is observed in the transition region. To investigate the boundary-layer state on the nozzle-exit conditions, pipe extensions are attached to the end of the SMC000 nozzle to generate boundary layers in laminar, transitional and turbulent states at the nozzle exit. It is found that the downstream jet plume affects the nozzle-exit boundary-layer development, causing the transition occurs earlier than that would occur inside a pipe. The nozzle-exit boundary layers in the transitional state involve significantly larger turbulence intensities, similar to those observed in a highly disturbed but nominally laminar boundary layer at the nozzle exit shown in experiments. This may suggest that those highly disturbed but nominally laminar boundary layers are in the transitional state. However, the far-field noise data generated by the three types of boundary layers are needed to confirm if the boundary layers in the transitional state indeed generate more noise than the turbulent boundary layer.

ACKNOWLEDGEMENTS

The author is grateful to Drs Daniel Ingraham and James Bridges at NASA Glenn Research Center for their support of this work. The author also would like to thank Dr. Zaman at NASA Glenn Research Center for the valuable discussions. Computing resources have been provided by the DoD High

Performance Computing Modernization Program Office. The meshes are generated by using an open source mesh generator GMSH (Ref. [22]).

REFERENCES

[1]. Zaman, K. B. M. Q., "Effect of initial condition on subsonic jet noise," AIAA J., Vol. 23, No. 9, 1985, pp. 1370–1373. doi:10.2514/3.9094.

[2]. Zaman, K. B.M. Q., "Effect of initial boundary-layer state on subsonic jet noise," AIAA J., Vol. 50, No. 8, 2012, pp. 1784–1795. doi:10.2514/1.J051712.

[3]. Viswanathan, K., and Clark, L. T., "Effect of nozzle internal contour on jet aeroacoustics," Int. J. Aeroacoust., Vol. 3, No. 2, 2004, pp. 103–135. doi:10.1260/1475472041494819.

[4]. Bogey, C., and Sabatini, R., "Effects of nozzle-exit boundary-layer profile on the initial shear-layer instability, flow field and noise of subsonic jets," J. Fluid Mech., Vol. 876, 2019, pp. 288–325. doi:10.1017/jfm.2019.546.

[5]. Bogey, C., and Marsden, O., "Simulations of initially highly disturbed jets with experiment-like exit boundary layers," AIAA J., Vol. 54, No. 4, 2016, pp. 1299–1312. doi:10.2514/1.J054426.

[6]. Liu, J., Corrigan, A., and Ramamurti, R., "Large-Eddy Simulations of Supersonic Jet Noise Generation Using Wall Modeling", presented at the Aviation meeting, June, 2018, Atlanta, Georgia. AIAA-2018-3943.

[7]. Liu, J., Ryan, R.F., and R., Ramamurti, "Numerical Study of Supersonic Jet Noise Emanating from an F404 Nozzle at Model Scale", 7-11 January 2019, San Diego, California. 10.2514/6.2019-0807.

[8]. Liu, J., Corrigan, A., Ryan, R.F., and R., Ramamurti, "Effect of Nozzle Inflow Conditions on Shock-Cell Structure and Noise in Overexpanded Jets", 25th AIAA/CEAS Aeroacoustics Conference, June, Netherland, doi: 10.2514/6.2019-2495.

[9]. Liu, J., Corrigan, A., and Kailasanath, K., "Equilibrium Wall-Model Implementation in a Nodal Finite Element Flow Solver JENRE for Large-Eddy Simulations", NRL Memo Report, NRL/MR/6040-17-9760.

[10]. Ingraham, D. J. and Bridges, J., " Validating a Monotonically-Integrated Large Eddy Simulation Code for Subsonic Jet Acoustics,"AIAA SciTech 2017. 10.2514/6.2017-0456

[11]. Bridges, J. and Wernet, M. P., \The NASA Subsonic Jet Particle Image Velocimetry (PIV) Dataset," Tech. Rep. NASA/TM 2011-216807, NASA Glenn Research Center, Cleveland, OH, United States, nov 2011.

[12]. Brown, C., and Bridges, J., "Small Hot Jet Acoustic Rig Validation," NASA Technical Memorandum, TM-2006-214234, National Aeronautics and Space Administration, 2006.

[13]. Bridges, J., and Brown, C., "Validation of the Small Hot Jet Acoustic Rig for Jet Noise Research,", AIAA Paper 2005-2846, AIAA, 2005.

[14]. Brown, C., "Jet-Surface Interaction Test: Far-Field Noise Results," Proceedings of the ASME Turbo Expo 2012, Copenhagen, Denmark, 2012.

[15]. Zaman, K.B.M.Q., "Increased Jet Noise Due to a "Nominally Laminar" State of Nozzle Exit Boundary Layer," NASA/TM—2017-219440, January, 2017.

[16]. Zaman, K. B. M. Q., "Exit Boundary Layer Data for a Round Convergent Nozzle in Support of Numerical Simulation Efforts", NASA/TM—2019-220242.

[17]. Stitch, G., Housman, J.A., Kocheemoolayil, J.G., Kiris, C.C. and Bridges, J.E., "Large-Eddy Simulation of Jet Surface Interaction Noise," AIAA Paper 2019-2475, 25th AIAA/CEAS Aeroacoustics Conference, May 20, 2019.

[18]. Boris, J.P., and Book, D.L., "Flux-corrected Transport I:SHASTA a fluid transport algorithm that works", Journal of Computational Physics, Volume 11. Issue 1. Pages: 38-69 (1973)

[19]. Löhner, R., Morgan, K., Peraire, J., and Vahdati, M., "Finite element flux-corrected transport (FEM-FCT) for the Euler and Navier- Stokes equations," International Journal for Numerical Methods in Fluids, Vol. 7, No. 10, 1987, pp. 1093–1109.

[20]. White, F.M., "Viscous Fluid Flow", McGraw-Hill Series in Mechnical Engineering, 1990.

[21]. Schlichting, H. and Gersten, K., "Boundary-layer theory", Spriger, 9th edition, 2017.

[22]. Geuzaine C. and Remacle, J. F., Gmsh: a three-dimensional finite element mesh generator with built-in pre- and post-processing facilities. International Journal for Numerical Methods in Engineering 79(11), pp. 1309-1331, 2009.

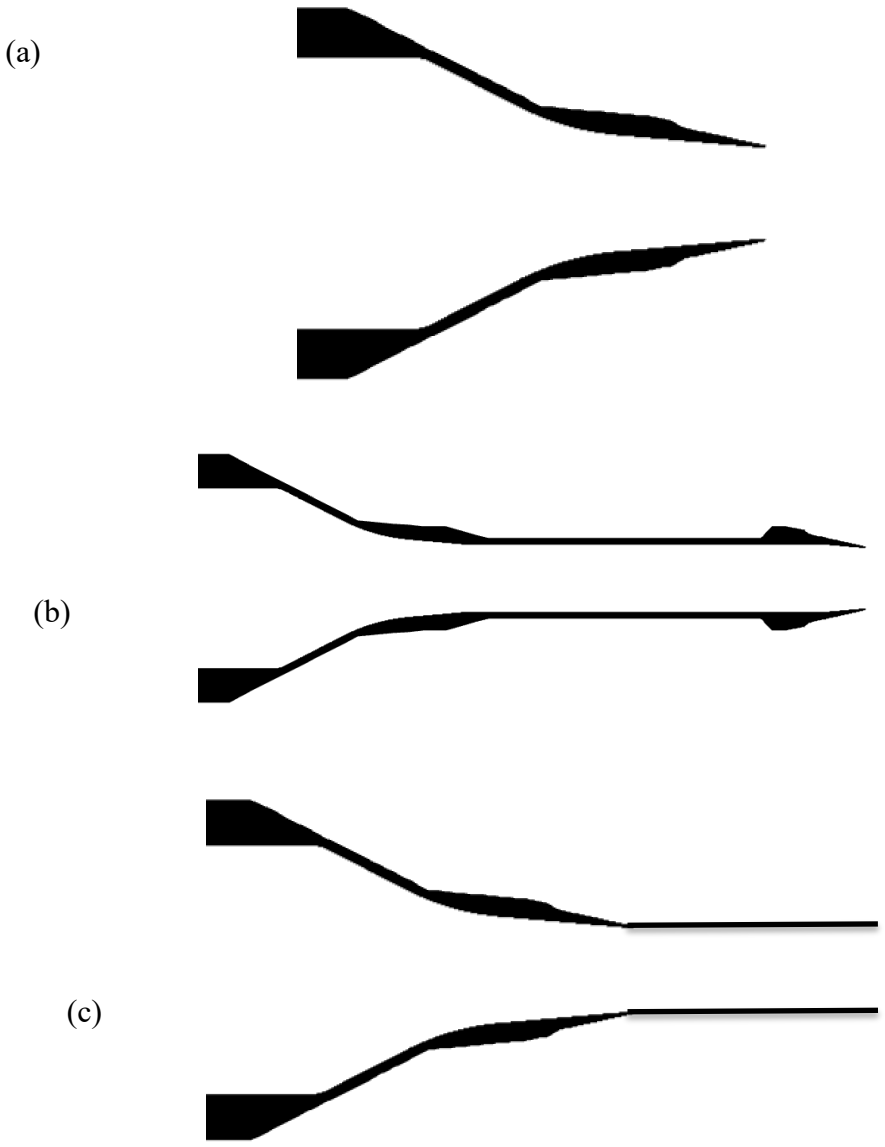

Figure 1. Nozzle geometries. (a). SMC000 nozzle. (b). Nozzle with a 12" pipe placed upstream of the final convergent section. (c). A pipe is attached downstream of SMC000 nozzle.

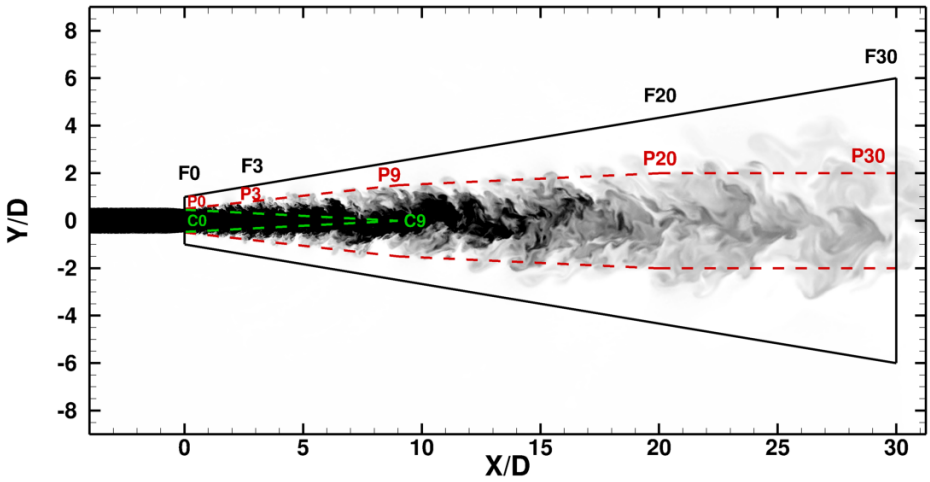

Figure 2. Computational domain. Parameters F0 to F30 and P0 to P30 are control points of cell sizes for jet plume and near-field region. The black solid lines are the location of FW-H surface for the far-field noise prediction. The specifications of those control points are given in Tables 1.

Table 1. Specifications of control points shown in Figure 2

Control Points	P0	P3	P9	P20	P30	F0	F3	F20	F30
Cell sizes	D/200	D/150	D/40	D/30	D/20	D/30	D/30	D/20	D/20
Radius	0.5D	0.69D	1.5D	2.0D	2.0D	1.0D	1.2D	4.3D	6.0D
Axial location	0D	3D	9D	20D	30D	0D	3D	20D	30D

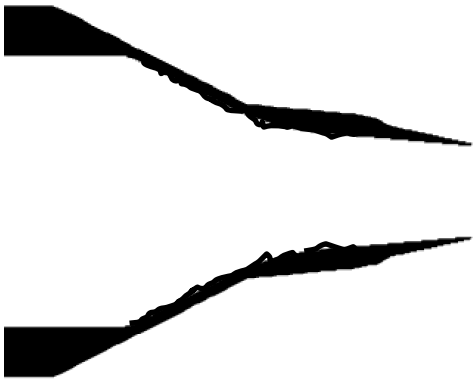

Figure 3. Surface roughness is added on the nozzle surface prior to the location one diameter upstream of the nozzle exit.

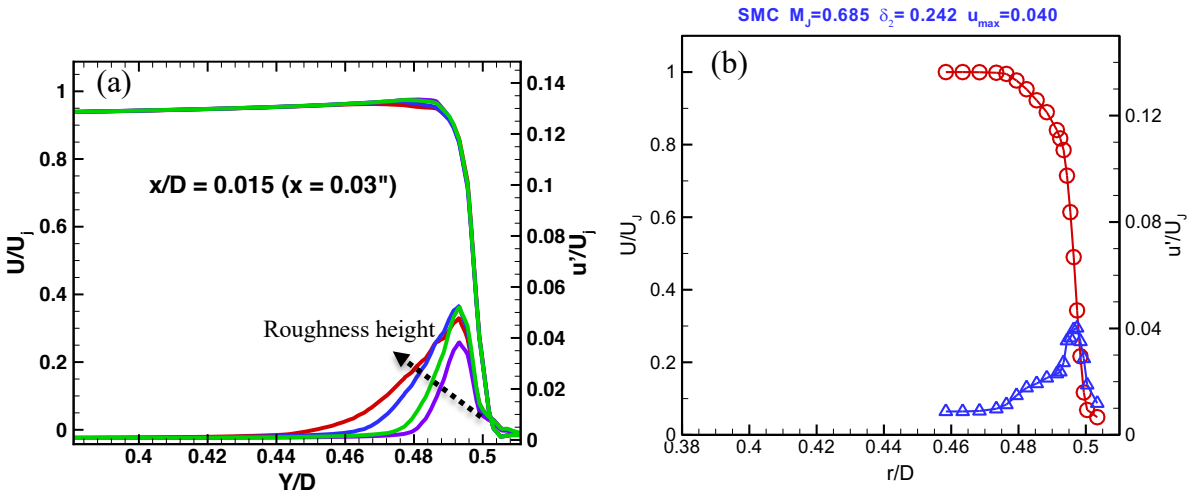

Figure 4. The impact of the roughness height on the nozzle-exit velocity and turbulence intensity profiles in jet flows with the acoustic Mach number $M_a = 0.7$ and $M_j = 0.736$. The SMC000 nozzle is used. The acoustic Mach number is the ratio between the velocity and the ambient sound speed. (a) LES predictions. Surface roughness heights are 1.0E-04", 6.7E-05", 5.9E-05" and 5.6E-05", respectively. (b) Experimental data at $M_j = 0.685$ [16].

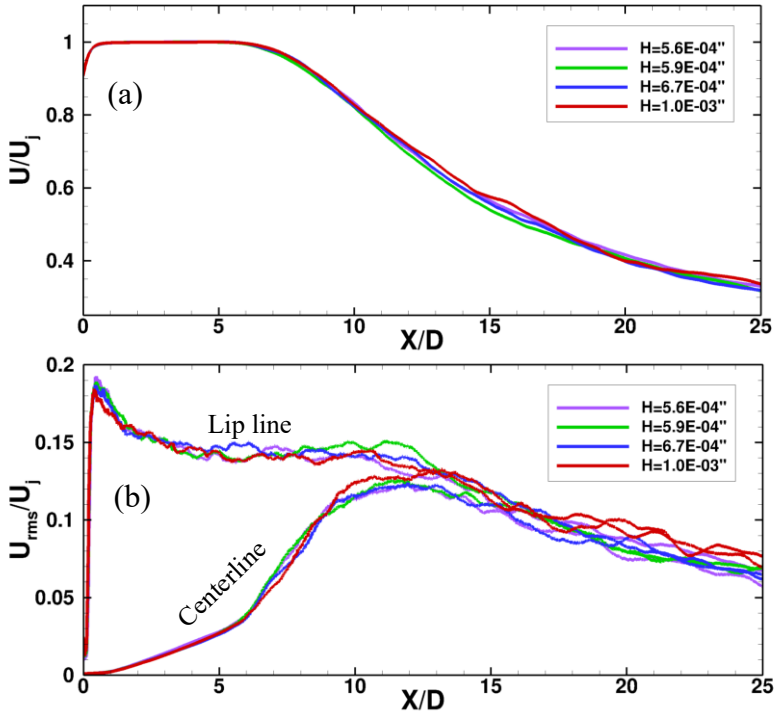

Figure 5. Axial velocity and turbulence intensity distributions of jet flows with an upstream boundary-layer tripping in the form of the surface roughness with various roughness heights. (a) Axial velocity along the centerline. (b) Turbulence intensity along the centerline and the lip line. Ma = 0.7 and M_j = 0.736 from SMC000 nozzle.

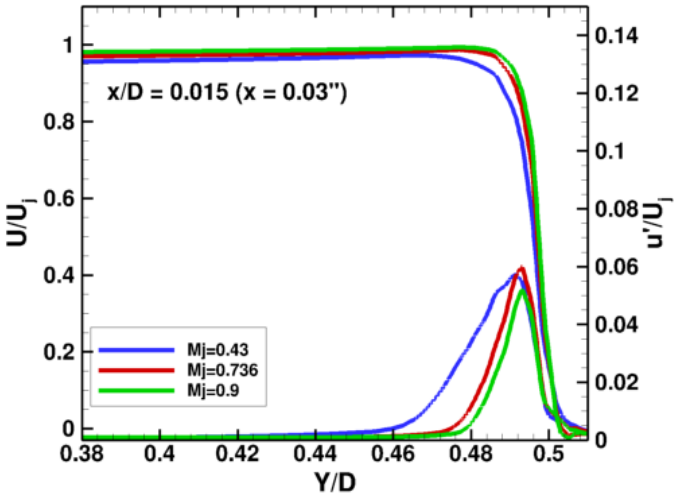

Figure 6. The effect of the jet Mach number on the nozzle-exit velocity and turbulence intensity profiles generated by the SMC000 nozzle.

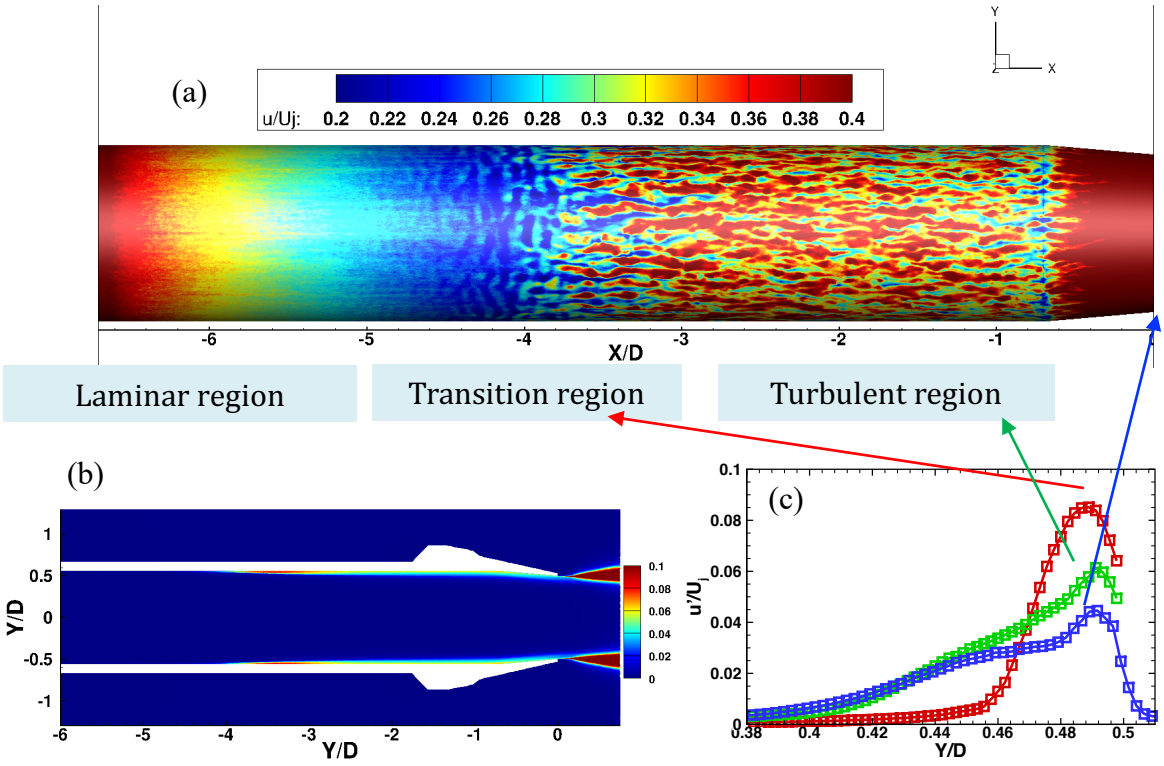

Figure 7. Turbulence structures, turbulence intensity contours and radial profiles in the nozzle boundary layer where a 12" pipe is added upstream of the convection section. No upstream boundary-layer tripping is used. $M_a = 0.7$ and $M_j = 0.736$. (a) Instantaneous velocity fluctuations near the nozzle surface. (b) Turbulence intensity contours inside the nozzle boundary layer. (c) Turbulence intensity radial profiles at three axial locations. The red line is at x = -3.4D, the green line is at x = -1.0D and the blue line is at x = 0.015D.

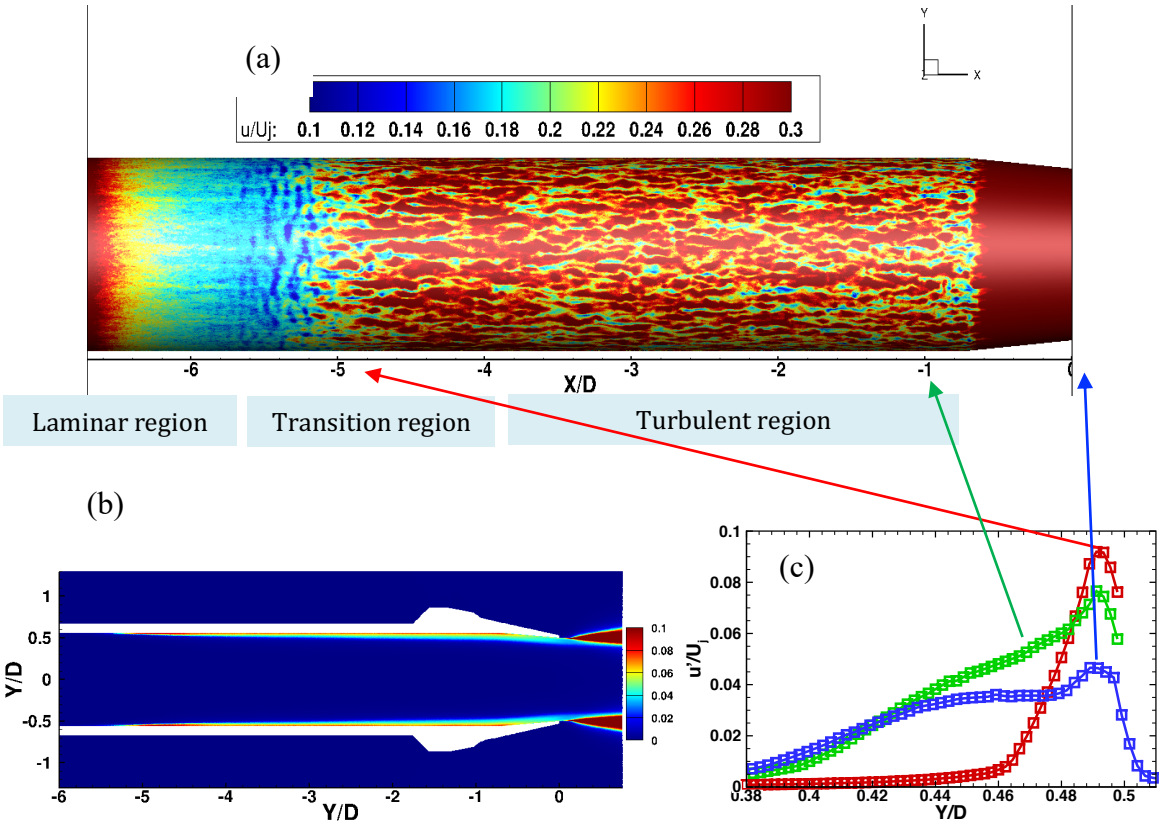

Figure 8. Turbulence structures, turbulence intensity contours and radial profiles in the nozzle boundary layer where a 12" pipe is added upstream of the convection section. Boundary-layer tripping is used upstream of the pipe. M_a = 0.7 and M_j = 0.736. (a) Instantaneous velocity fluctuations near the nozzle surface. (b) Turbulence intensity contours inside the nozzle boundary layer. (c) Turbulence intensity radial profiles at three axial locations. The red line is at x = -4.8D, the green line is at x = -1.0D and the blue line is at x = 0.015D.

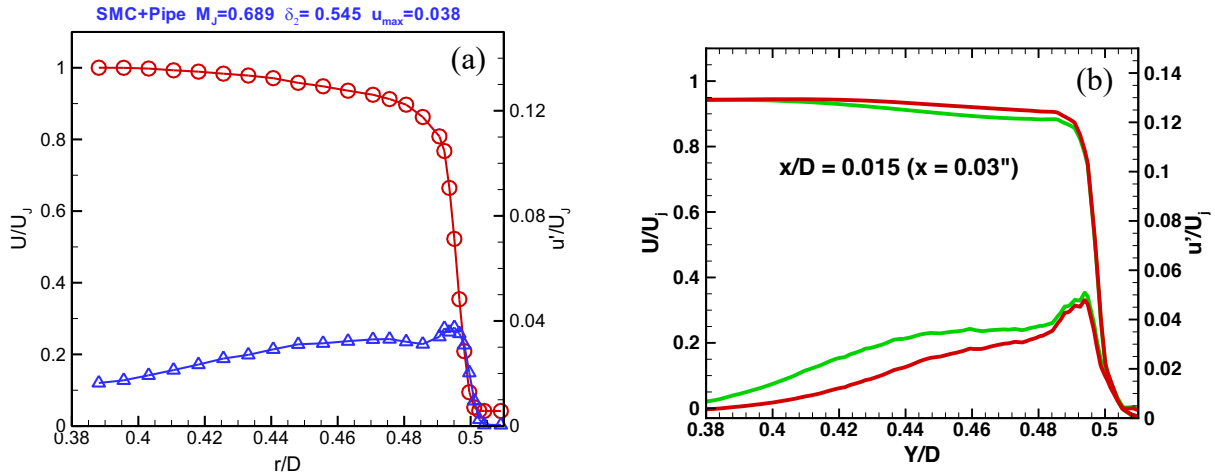

Figure 9. Nozzle-exit velocity and turbulence intensity profiles generated by the nozzle with a 12" pipe attached upstream of the convergent section. (a) Experimental data at M_j = 0.689. (b) LES predictions with (green lines) and without (red lines) boundary-layer tripping upstream of the 12" pipe. The acoustic Mach number M_a = 0.7 and the jet Mach number M_j = 0.736.

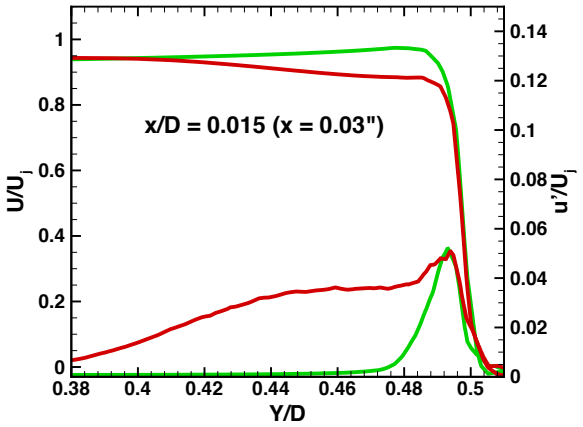

Figure 10. Comparison of the nozzle-exit velocity and turbulence intensity profiles generated by the SMC000 nozzle and the nozzle with 12" pipe upstream of the final convergent section. The acoustic Mach number Ma = 0.7 the jet Mach number M_j = 0.736.

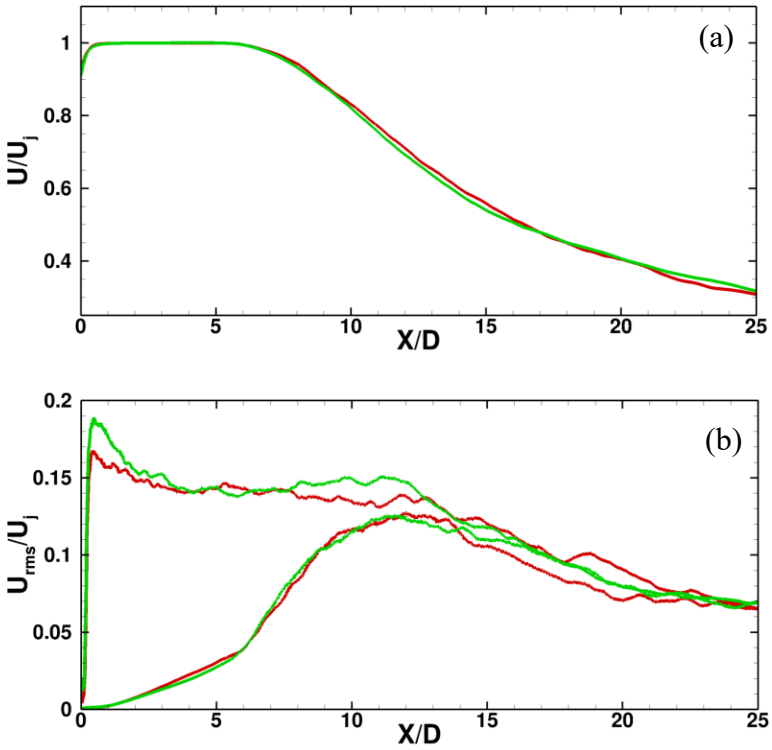

Figure 11. Axial velocity and turbulence intensity distributions. M_a = 0.7 and M_j = 0.736. Red lines: A 12" pipe is added upstream of the final convergent section of the SMC000 nozzle and a boundary-layer tripping is added upstream of the pipe. Green lines: SMC000 with roughness added prior to the location one diameter upstream of the nozzle exit. The roughness height is 5.9E-4". (a) Axial velocity along the centerline. (b) Turbulence intensity along the centerline and the lip line.

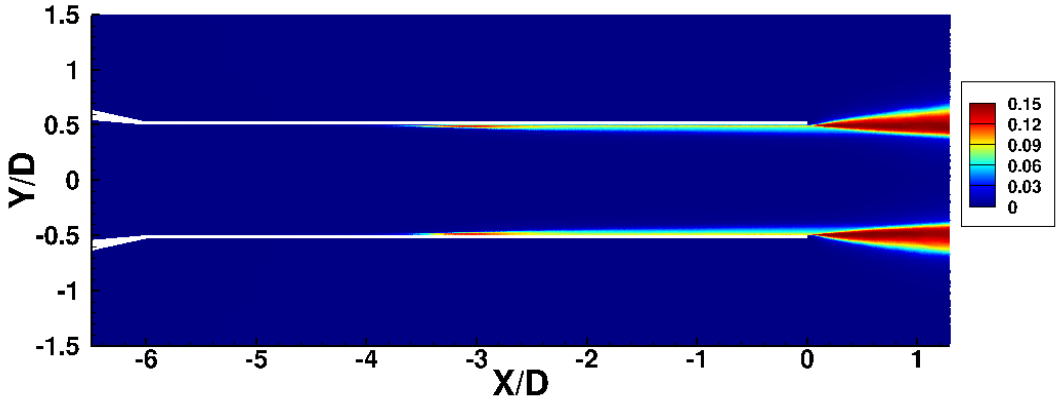

Figure 12. Turbulence intensity contours of the boundary layer inside the 12" pipe attached downstream of the SMC000 nozzle. The jet Mach number $M_a = 0.7$ and $M_j = 0.736$.

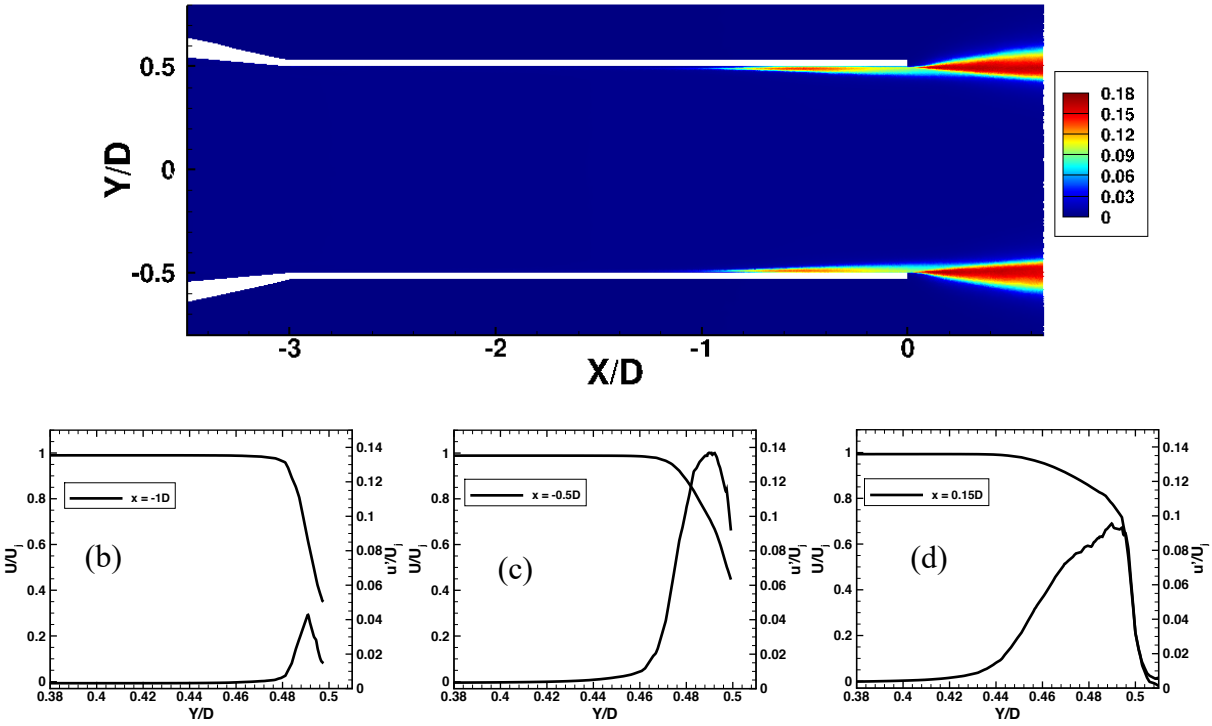

Figure 13. Turbulence intensity contours and the radial profiles of a jet flow at $M_a = 0.7$ and $M_j = 0.736$ from the nozzle with a pipe attached to SMC000 nozzle. The pipe length is 3D. (a) Turbulence intensity contours inside the nozzle. Radial profiles of the axial velocity and turbulence intensity at (b) x = -1.0D, (c) x = -0.5D, and (d) x = 0.015D.

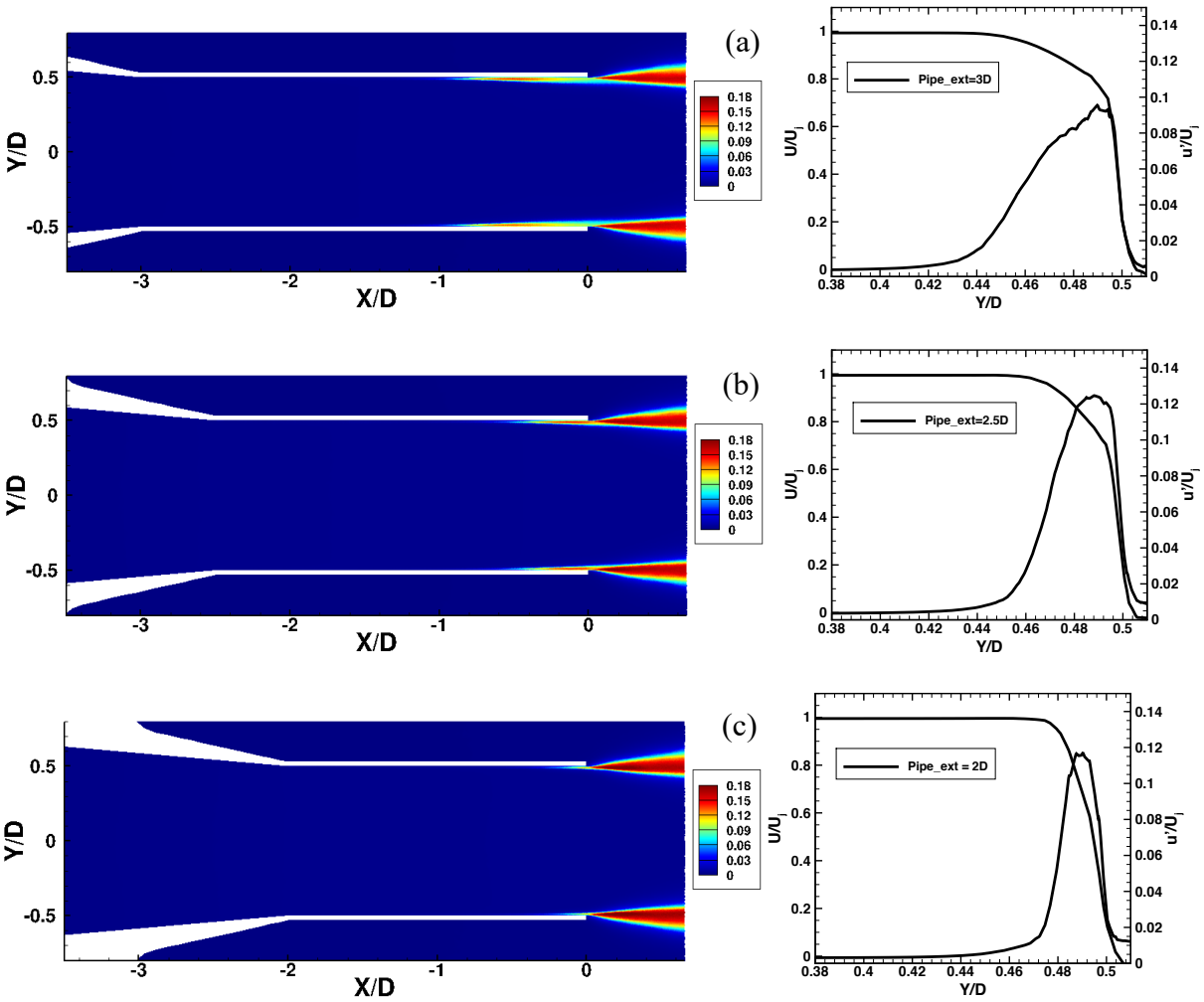

Figure 14. Turbulence intensity contours and the radial profiles of jet flows at M_a = 0.7 and M_j = 0.736 from the nozzles with a pipe attached to the SMC000 nozzle. Three pipe lengths are tested and the attached pipe length is (a) 3D (b) 2.5D (c) 2D. The figures on the left are turbulence intensity contours and plots on the right are the radial profiles at x = 0.015D.

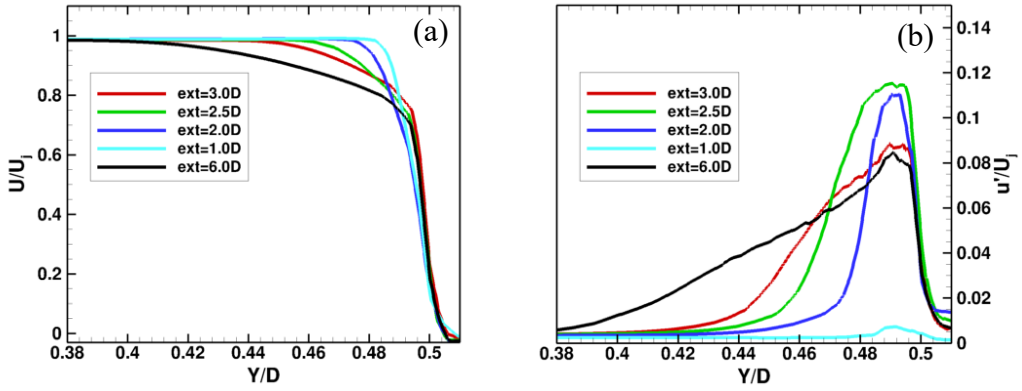

Figure 15. Nozzle-exit profiles of nozzles where pipes with various lengths are attached to the SMC000 nozzle. The jet condition is M_a = 0.7 and M_j = 0.736. (a) Velocity profiles. (b) Turbulence intensity profiles.

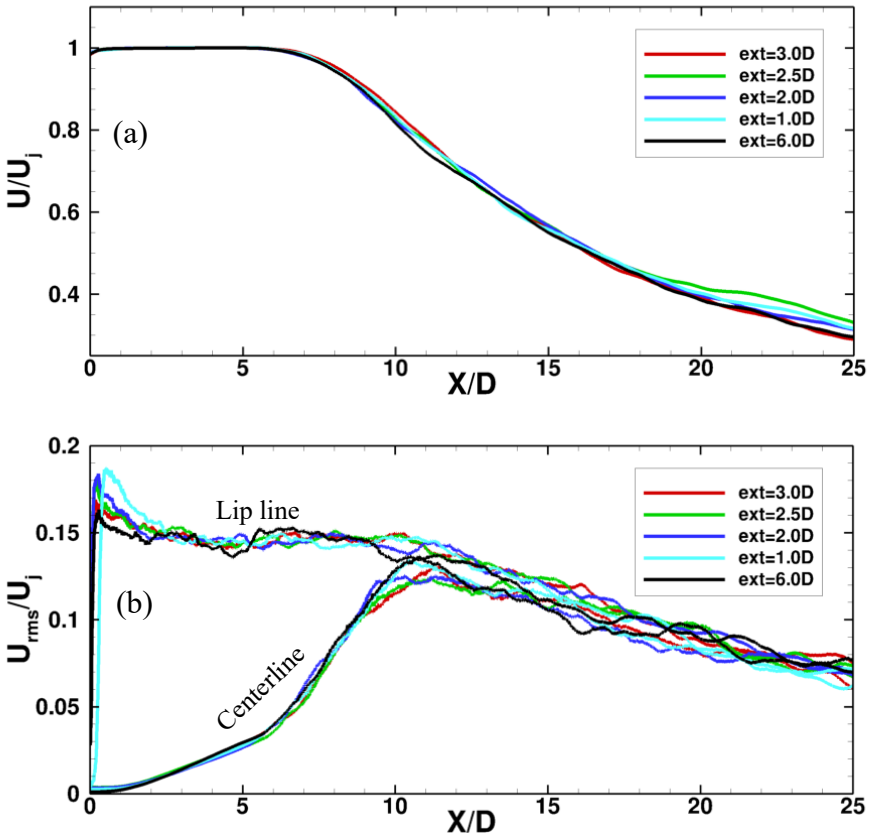

Figure 16. Axial distributions of the axial velocity and turbulence intensity of nozzles where the SMC000 nozzle is attached with a pipe of various lengths. The acoustic Mach number is $M_a = 0.7$ and the jet Mach number is $M_j = 0.736$. (a) Axial velocity along the centerline. (b) Turbulence intensity along the centerline and the lip line.

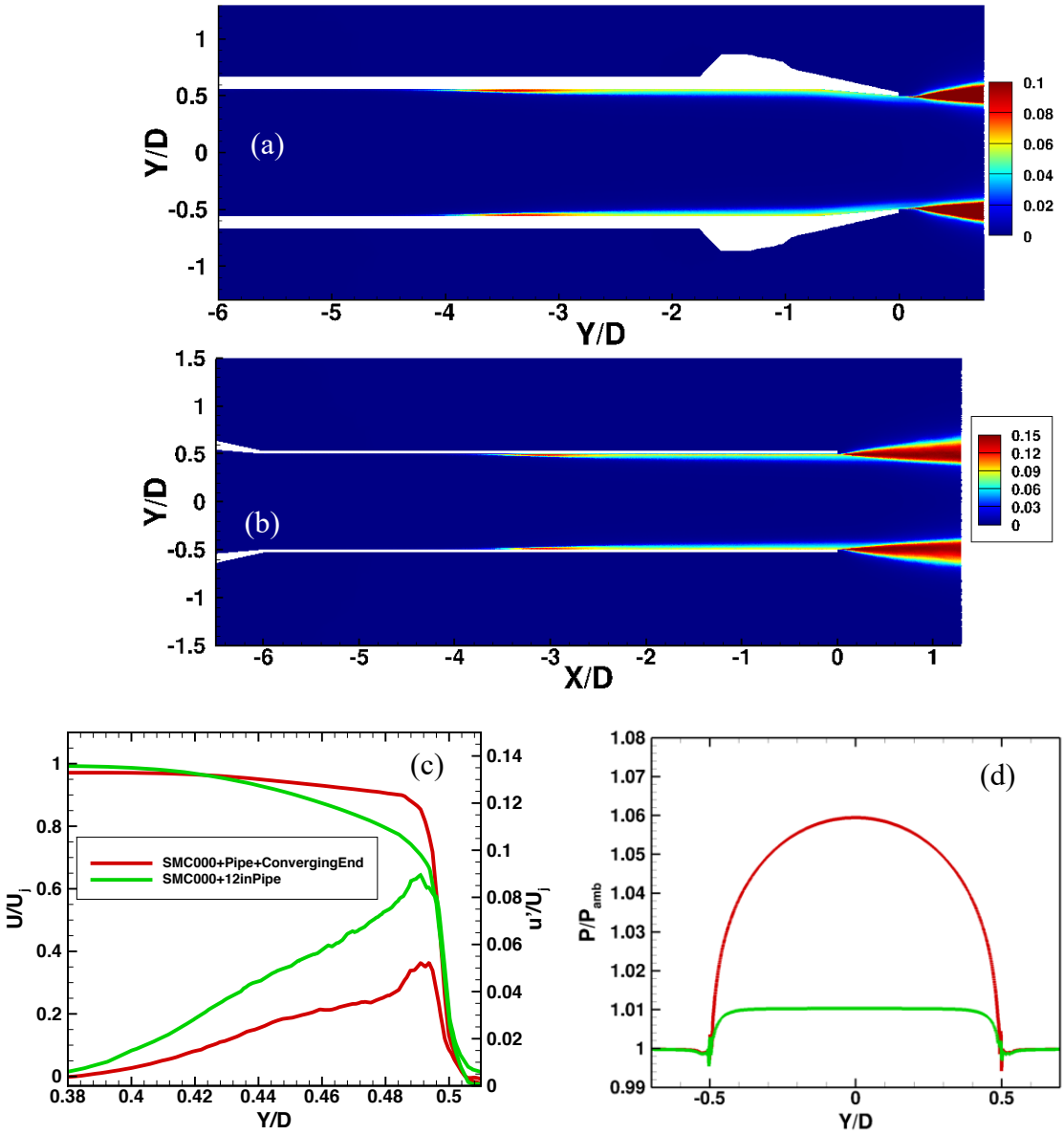

Figure 17. Comparison of the turbulence intensity contours inside the nozzle and the nozzle-exit radial profiles generated by two types of nozzles. (a) Turbulence intensity contours of the nozzle where a pipe of 12" length is used upstream of the convergent section. (b) Turbulence intensity contours of the nozzle where a pipe of 12" length attached to the SMC000 nozzle. (c) Radial profiles of the axial velocity and the turbulence intensity near the nozzle exit at x = 0.015D. (d) Radial profiles of the pressure normalized by the ambient pressure near the nozzle exit at x = 0.015D.